A Novel Method of Frequency Regulation in Microgrid

Upama Bose, *Student Member, IEEE,* Sumit K Chattopadhyay, *Member, IEEE,*
Chandan Chakraborty, *Fellow, IEEE,* and Bikash Pal, *Fellow, IEEE*

***Abstract*—Owing to generation and demand mismatch, the frequency deviation and the rate of change of frequency (RoCoF) may become drastic at times in an islanded micro-grid. This is due to increased penetration of non-inertial renewable energy sources that brings down the system's resilience to any kind of disturbance. Therefore, efficient control algorithms are required to mimic the inertial behavior of a conventional synchronous machine to arrest/limit any sudden change. This work focuses on frequency regulation of microgrid during transient conditions by means of fast-responding external energy reserve. The characteristics of a weak grid has been studied and simulated through modeling a Virtual Synchronous Machine (VSM). An inverter model is also developed to integrate the Energy Storage System (ESS) to the grid and a Double Second-Order Generalized Integrator Phase Locked Loop (DSOGI-PLL) is implemented that is capable of synchronizing the system under distorted and unbalanced situation. A new technique to estimate the frequency of the microgrid is reported. A simple proportional controller based approach for different level of pulsed power injection (using ultracapacitors and batteries) is proposed and simulated using MATLAB. Experimental demonstration is made using batteries only but with two different current-limits. The controller is implemented using dSPACE1103.**

***Index Terms*—Virtual Synchronous Machine (VSM), Frequency Regulation, Microgrid Dynamics, Energy Storage System (ESS), Synthetic Inertia, Rate of Change of Frequency(RoCoF), Renewable Energy Integration**

NOMENCLATURE

J	Combined moment of inertia of generator and turbine.
ω_m	Mechanical angular velocity
ω_r	Electrical angular velocity
ω_o	Nominal frequency
T_a	Accelerating torque
T_m	Mechanical torque
T_e	Electromagnetic torque
D	Damping constant
P_m	Mechanical power
P_e	Electrical power
P_o	Nominal power
k_p	Droop constant
m_a	Modulation index
i_d	d-axis inverter current
i_q	q-axis inverter current
$i_{d_{ref}}$	Reference d-axis inverter current
$i_{q_{ref}}$	Reference q-axis inverter current
P_{ess}	Rating of ESS-inverter
J_{nom}	Nominal value of inertia (J) of VSM

Manuscript received December 30, 2017; revised March 22, 2018 and June 19, 2018; accepted August 2, 2018.

This work is supported by Department of Science & Technology (DST), India through a project entitled UK India Clean Energy Research Institute (UKICERI) (DST/RCUK/JVCCE/2015/02 (C)), and EPSRC funded Joint Clean Energy Research Centre (JUICE) (EP/P003605/1) which is a joint collaboration initiative between DST, India and EPSRC, UK.

Upama Bose and Chandan Chakraborty are with the Department of Electrical Engineering, Indian Institute of Technology Kharagpur (e-mail: upama16@gmail.com; chakraborty@ieee.org)

Sumit K Chattopadhyay is with the Centre for Energy Studies, Indian Institute of Technology Delhi (e-mail: sumitkc1981@gmail.com)

Bikash Pal is with the Department of Electrical and Electronic Engineering, Imperial College London, SW7 2BT,London (e-mail: b.pal@imperial.ac.uk)

Digital Object Identifier "**********"

I. INTRODUCTION

Global climate change concerns have put emphasis on alternative energy sources. However, the grid-penetration of renewable energy sources, such as Solar PV or Wind energy system, which are increasingly replacing the conventional power plants based on large synchronous generators, leads to a reduction of the total inertia of the system. While generators used in the wind-electric power conversion still have the inertia-factor, the solar PV is practically devoid of such property. Both are, however, connected through power electronic interface, the overload capability of which acts as a final limiting factor. As a consequence, higher rate of change of frequency (RoCoF) can be observed during sudden and large disturbances in the system (either due to fault, or sudden disconnection/collapse of large generator or connection/disconnection of large load in the system). Therefore, there is a strong motivation for improving the way in which the power system with low inertia could provide primary frequency restoration.

During the last decade, several concepts for Virtual Synchronous Machines (VSMs) have been presented with different names and different practical implementations. Virtual inertia is the concept of mimicking inertial behavior of a traditional generator system. In [1], a detailed nonlinear mathematical model for this VSM implementation has been derived. The time domain behavior of synchronous machines, in terms of inertia response and damping, is modeled by the traditional swing equation [2]. The amount of virtual inertia that can be added to the system by a single VSM unit can also be realized by proper energy storage systems [3]. On the other hand, [4], [5], [6] describe the advantage of the short response time (in milliseconds) of modern Energy Storage Systems (ESS) to improve the dynamic performance of isolated power systems just after a sudden imbalance between generation and demand. For that the sizing of the energy storage elements has to be

properly calculated depending on how much dynamic support is required and for how long. Reference cited in [7] introduces the aspect that the primary frequency control depends on the relation between frequency & State of Charge (SoC) of the energy storage while the secondary control changes power output depending on the frequency signal. It has been shown in [8], [9] that the amount of inertia supplied by the inverter-based source operating with traditional droop can be neglected, whereas inverter-based sources contribute mostly to damping of electromechanical modes. Electromechanical modes of synchronous generator based sources and power modes of inverter-based sources are critical for system stability. A Virtual Synchronous Machine-based Electric Vehicle charger [10] is shown to contribute to the spinning reserve and the frequency regulation of the power system. The control strategy described in [11] combines the effect of swing equation in the modification of the conventional droop control. This results in reduction of not only the RoCoF (rate of change of frequency), but also the maximal deviation of frequency with respect to the nominal value. Here, the RoCoF depends on the value of the chosen virtual inertia. So, to limit the rate of change of frequency to a decent value, much higher value of virtual inertia constant should be chosen. Apart from VSM, in another control methodology, the output power of the PV generator itself is controlled to maintain the system frequency by keeping some portion of the PV output as reserve [12]. This can eliminate the usage of costly storage units like battery. De-loading the PV, i.e. operation below maximum power point (MPP) to provide reserve is an economical solution. However, a trade-off lies between the cost of additional PV unit having the reserve features in-built and cost of battery unit. Also, de-loading of PV reserve is not an optimum solution. Reference [13] introduces how virtual inertia can be emulated through DC-link voltage control and PV array generation adjustment. Improved control techniques for providing frequency support in wind farms through synthetic inertial behaviour, are also reported in some of the recent literature. Few can be pointed out as Wind Turbine Generators level torsional oscillation damping control, low frequency oscillation adaptive damping control to enhance damping characteristic of the Wind Farm (WF) [14] and Linear Quadratic Regulator to obtain the optimum control trajectory [15]. Some researchers have also focused on injecting virtual inertia by means of adding Lithium-ion supercapacitors in the DC link of the doubly-fed induction generator (DFIG) power electronic conversion system to increase extra energy storage capability [16]. Some authors have proposed inertia emulation from electro-static energy stored in the DC-link capacitor of high-voltage direct current (HVDC) system [17], [18], [19]. The inertia constant has been derived from the analogy of the electro-static energy stored in the DC-link capacitor with that of the kinetic energy stored in the rotating masses of the synchronous generator. However, to derive synthetic inertia from these methods, large capacitor size and wider range of dc-bus voltage margin should be ensured. Reference [20] utilizes Energy Storage System (ESS) for proving short-term active power support, particularly for preventing load shedding due to transient declines in frequency. Reference [21] proposes the option to use different energy storage mix to combat frequency deviation problem.

This paper proposes a new frequency regulation concept for a stand-alone microgrid. For such purpose, a simple microgrid, having one VSM, one load and an ESS-fed inverter, is considered. When there is change in load (decrease/increase), the frequency undergoes quick variation, even in case of system with high inertia. This is of course severe for low inertia systems. Hence, it is extremely important to fast estimate the grid frequency. All methods (standard Phase Locked Loop (PLL) techniques, Kalman filter, etc) proposed so far are computation-intensive and those are also not able to estimate frequency sufficiently quickly. In this paper, a new frequency estimation technique is proposed, simulated and experimentally validated. Frequency regulation and restoration are done through active power control. This is demonstrated in this work by injecting pulse active power in proportion to the frequency deviation by means of a simple proportional control mechanism. The provision of having multiple type energy storages (of different time-scales) is also discussed. The paper is organized as follows: Section I introduces the motivation and challenge associated with frequency regulation in microgrid. Section II describes the system configuration and modeling. The controller structures are shown in section III. The simulation platform is developed in MATLAB/Simulink and the results are shown and discussed in section IV. Experimental validation is carried out efficiently which is an extended version of the work shown in [22] which is presented in section V. The results clearly show the effectiveness of the control algorithm.

II. Proposed System Description

A. Schematic Representation of the overall system

The motivation of the work is to improve the frequency regulation of the microgrid. A stand-alone grid having low inertia is considered. In view of this, the system is modeled

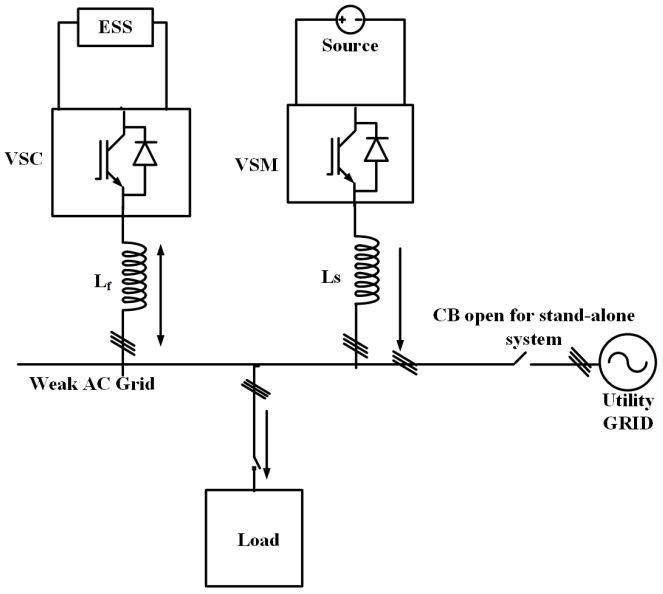


Fig. 1. System Configuration

by a Synchronous Machine (SM) programmed as Virtual Synchronous Machine, a parallel Energy Storage connected inverter and load. The modeling of VSM adds flexibility to the system to work with various ratings and inertia constants (J) of SMs or diesel generator without an actual machine which would have been a limitation. The inverter is paralleled with the synchronous machine with the help of PLL synchronization. Considering the fact that a micro-grid is prone to occurrence of unbalances and disturbances, a DSOGI-PLL [23] is used for the purpose. The system configuration is shown in Fig. 1. The virtual synchronous machine is implemented in simulation and laboratory prototype by using a dc source and a corresponding three-phase Voltage Source Converter (VSC). VSM rating is chosen same as the maximum load demand of the system considered, whereas the power rating of the ESS-inverter is so chosen to emphasize the fact that the ESS-inverter should be used to handle the transient pulsed power just at the instant of a load change to arrest the sudden large frequency deviation and also the rate of change of frequency (RoCoF).

In steady-state condition, the power delivered by the inverter connected to the energy storage reduces to zero; meanwhile, the VSM can take up all the load power. In this way, the frequency regulation in a microgrid due to a disturbance from the load-side, can be efficiently dealt with.

B. VSM modeling

The emulation of the VSM is based on the conventional swing equation of a synchronous machine, combined with the equation of droop mechanism. The basic equation of motion is as follows [24]:

$$J\frac{d\omega_m}{dt} = T_a = T_m - T_e - D\omega_m \tag{1}$$

As the motivation here is to study the effect of inertia, the influence of damping is neglected. Now, considering a 2-pole machine, the following simplified equation can be written:

$$J\omega_r\frac{d\omega_r}{dt} = P_m - P_e \tag{2}$$

On the other hand, the operating principle of droop control can be described by the following equation [25]:

$$\omega_r = -\frac{1}{k_p}(P_e - P_o) + \omega_o \tag{3}$$

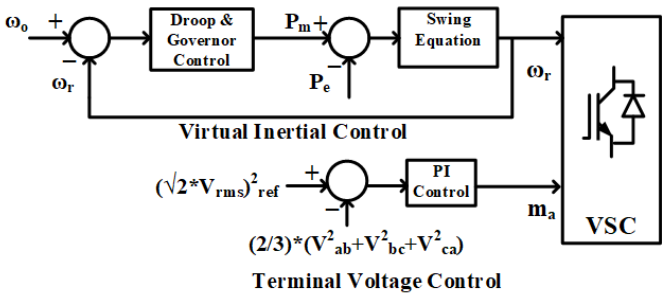


Fig. 2. Control diagram of VSM

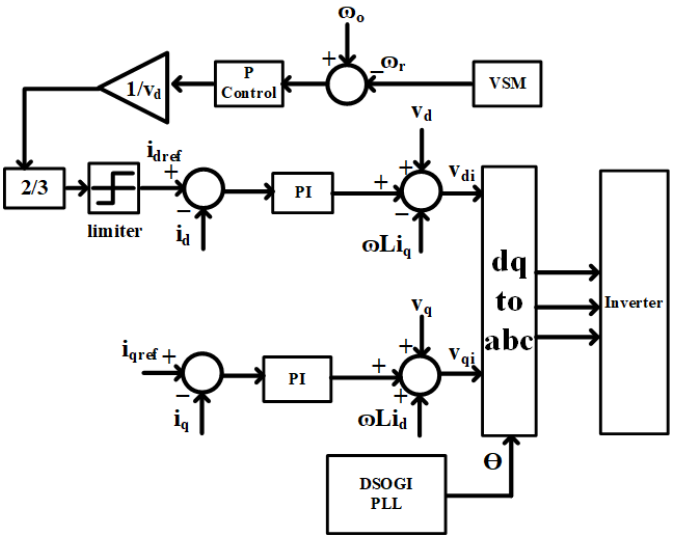


Fig. 3. Decoupled current control of ESS-inverter

Now, combining the conventional droop equation and the swing equation, the following equation governing the VSM-dynamics can be obtained:

$$J\omega_r\frac{d\omega_r}{dt} = P_o + k_p(\omega_o - \omega_r) - P_e \tag{4}$$

where,

$$P_m = P_o + k_p(\omega_o - \omega_r) \tag{5}$$

III. Controller Structures

A. VSM Control Strategy

The block diagram shown in Fig. 2 depicts the control strategy of inertia emulation of the power converter modeled to behave like that of a conventional synchronous machine. The controller includes the inertia algorithm which is executed in the form of a swing equation [26]. The droop control and governor action are responsible for frequency control. In this way the control strategy acts for restoring the frequency back to nominal value after a sudden drop for any increase in load. The terminal voltage control is performed by the VSM controller as shown in Fig. 2. The generated frequency, ω_r serves as the fundamental frequency reference for the inverter; the nominal frequency considered in this study is $2 * \pi * 50$ rad/s and m_a is the reference modulating signal. These two parameters are used to generate reference for the PWM of the VSC switches.

B. ESS-inverter Control Strategy

The scheme used here to control the ESS-inverter is Voltage Oriented Controlled (VOC) [27], commonly known as 'p-q control'. The term 'p-q control' indicates the independent control of active and reactive power of the inverter by means of decoupled control of d-axis and q-axis currents. This is based on transformation between abc and dq frames. For implementing this control strategy, the load voltage is measured and the

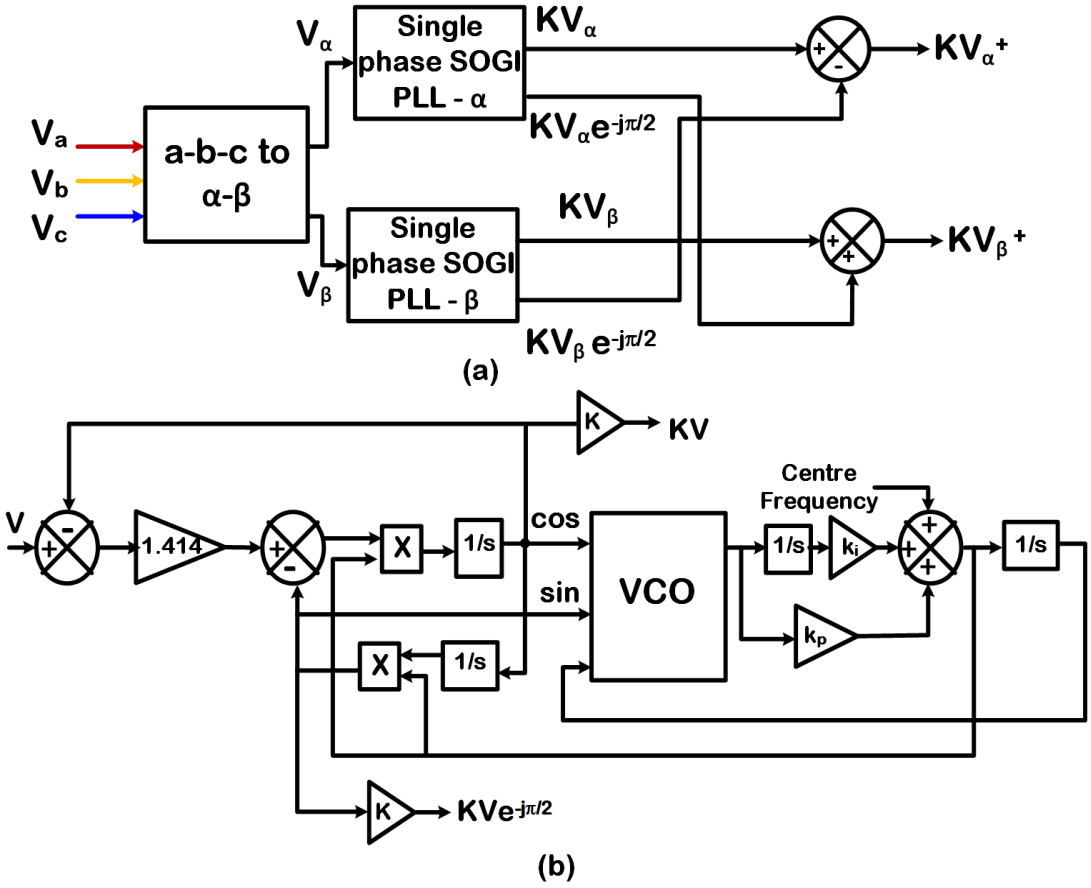


Fig. 4. DSOGI PLL: (a) Overall block diagram, (b) Detailed diagram for single phase SOGI PLL-α and SOGI PLL-β blocks

instantaneous phase angle of the voltage vector is detected using PLL for voltage orientation. This angle is used for the transformation between reference (abc to dq and vice versa) frames. Practically, the load voltage, especially, in a microgrid, may contain harmonics and unbalances. That is why DSOGI-PLL model [23] is used in this case for synchronization purposes. The load voltage vector is aligned with the d-axis, resulting the q-axis component of the load voltage vector to be zero. This action is performed by the DSOGI-PLL, taking account of the positive and negative sequence voltages that can result from unbalances. The implementation diagram of DSOGI-PLL is displayed in Fig. 4 and the corresponding parameters are listed in Table I. With this VOC strategy, the three-phase line currents of the ESS-inverter are measured and transformed into d and q components. The decoupled control of these two components, i_d and i_q renders an effective means to independently control the active and reactive power-flows, respectively. These, i_d and i_q, are compared with, $i_{d_{ref}}$ and $i_{q_{ref}}$ and the errors are fed to corresponding PI controllers. The output of the PI controllers, with feed forward terms, generates the voltage reference for the dedicated converter used with energy storage for frequency stabilization as shown in Fig. 3. This controller is activated only during the event of frequency fluctuation till its restoration to allowable range.

1) Frequency Controller: The d-axis current reference, $i_{d_{ref}}$, which represents the active power to be fed by the ESS-converter system, is generated by a proportional controller. This performance of the ESS-inverter is similar to injecting synthetic inertia into a weak grid. The amount of pulsed power injection based on frequency deviation is determined by a high gain proportional controller. This helps to avoid the oscillatory response usually observed due to multiple PI controllers in a given system. Though it is possible to improve the system dynamics by properly tuning the PI controllers, however, it is difficult to completely mitigate the system oscillations. Also it is important to note that, even if the ESS inverter would have been controlled by a properly tuned PI controller, it would continue to inject certain amount of power in steady-state due to the integral part of the controller. In that case, some additional suitable control action is necessary to smoothly ramp down the integrator output to zero once frequency is restored within the acceptable range. In the proposed controller only a proportional constant is enough to solve the above mentioned issue. Thus, due to any mismatch between generation and

TABLE I
DSOGI PLL PARAMETERS

System Parameters	Values
Centre frequency	50 Hz
Gains of PI controller	k_p=500, k_i=100
Constant (K)	-0.5

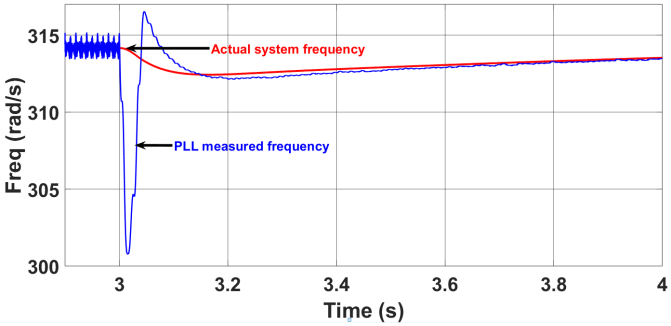


Fig. 5. System frequency measurement by DSOGI-PLL

demand, if there is any frequency drop, the frequency control loop is activated and a proportionate active power reference is generated by the proposed controller to mitigate the sudden frequency change.

Here, it is assumed that the speed feedback from the VSM can directly be fed to the ESS-inverter for power flow control. The motivation behind taking the speed feedback from the VSM to estimate the system-frequency comes from the observation that frequency measurement method by observing the grid voltage (using PLL) demands few cycles to accurately detect frequency change because of PLL's own dynamics and controller gains. This frequency tracking gets more delayed in a microgrid due to higher distortion in the grid voltage. For example, a well-tuned second-order generalized integrator phase locked loop (SOGI-PLL) with parameters given in Table I with its block diagram illustrated in Fig. 4 will have frequency response as shown in Fig. 5. Clearly, it can be seen that the PLL adds finite amount of delay to synchronize. This delays the frequency control action to such an extent that frequency regulation through frequency estimation using PLL becomes impossible during transient conditions. That is why the measured speed from VSM controller is used for generating the active power reference to regulate the frequency. This speed gives corresponding information of the system-frequency. Hence, the frequency response is improved by proper transient power handling capability of the ESS-converter. Once the frequency restoration starts from the frequency controller of the VSM, the active power fed by the ESS-converter starts to decrease and that of the VSM rises. In steady state, when the frequency is brought back to nominal value, the power output of the ESS-inverter is settled at zero and in the process, VSM gradually takes up the total load demand.

IV. Simulation Results

Simulations have been performed in MATLAB/Simulink to verify the virtual inertia algorithm and also to test the controller for frequency regulation. The system parameters are listed in Table II. The dynamic behavior of the weak grid is observed by switching a 3 kW load to a generation system. The generation system consists of a 3 kVA virtual synchronous generator to emulate the inertial characteristics of a conventional alternator, in parallel with a voltage source converter connected to an energy reserve. To check the effectiveness of

TABLE II
Simulation System Parameters

System Parameters	Values
Sampling frequency	1 MHz
Switching frequency	2 kHz
PI gains of the governor (droop control) of VSM	k_p=200, k_i=1000
PI gains of grid voltage controller of VSM	k_p=0.001, k_i=0.01
Proportional gain of the proposed controller	k_p=6000
PI gains of the d-q current controllers	k_p=24, k_i=3200
Load voltage (line to line, rms)	110 V
Load	3 kW (resistive)
Filter inductors	9 mH
VSM rating	3 kVA
Nominal value of J	0.05 kg.m^2

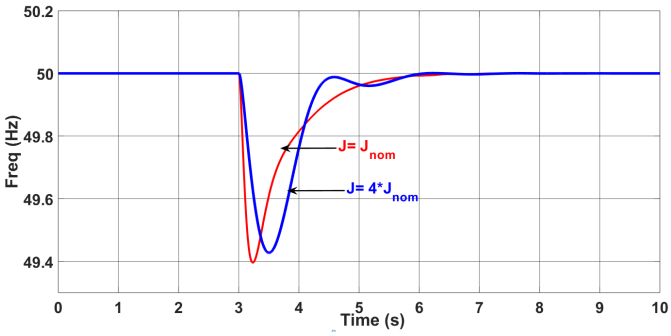


Fig. 6. Frequency dynamics of VSM

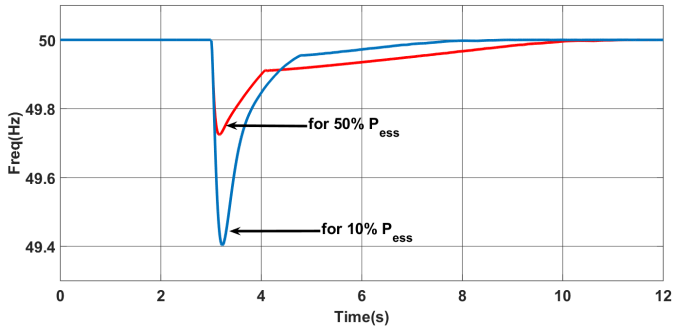


Fig. 7. Improved frequency dynamics due to proposed controller for different ratings of ESS inverter

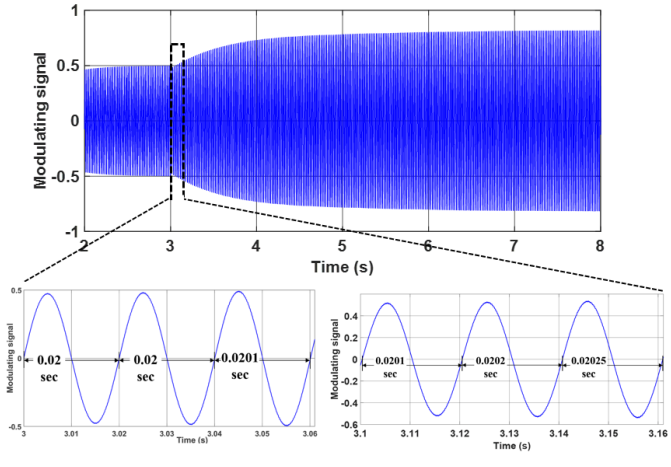


Fig. 8. Modulating signal m_a for VSM

TABLE III
EFFECT OF ESS-INVERTER RATING ON FREQUENCY RESPONSE

ESS-inverter Rating (as % of total load)	Freq Nadir (Hz)	RoCoF (Hz/s)	Peak Power handled (kW)	Peak Current (A)
10%	49.40	2.67	0.29	2.23
30%	49.55	2.04	0.87	6.68
50%	49.72	1.65	1.44	11.13

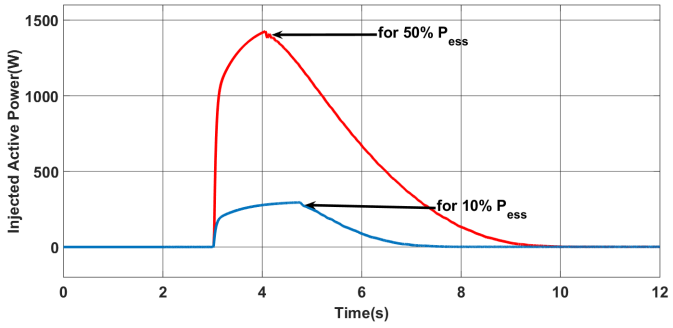


Fig. 9. Power Curve of p-q controlled ESS-inverter for different ratings

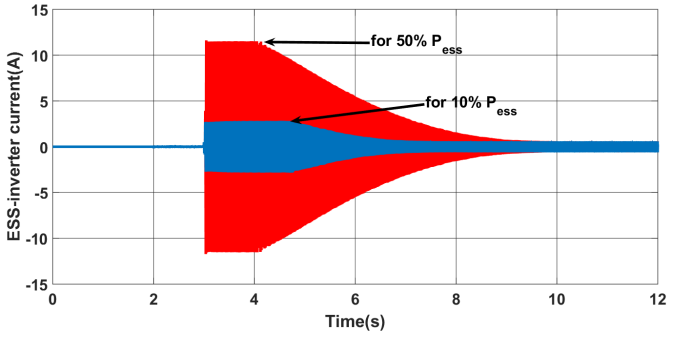


Fig. 10. Maximum current handled by p-q controlled inverter for different ratings

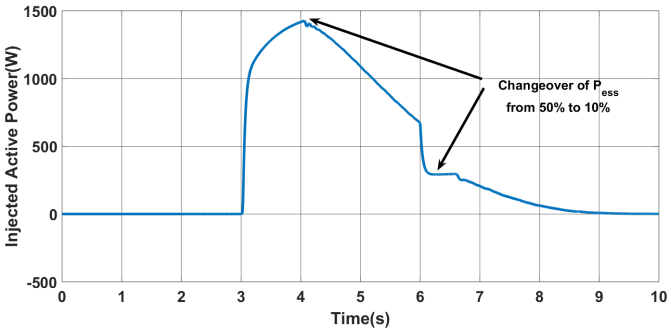


Fig. 12. Peak power handled by p-q controlled inverter during changeover of rating from 50% to 10%

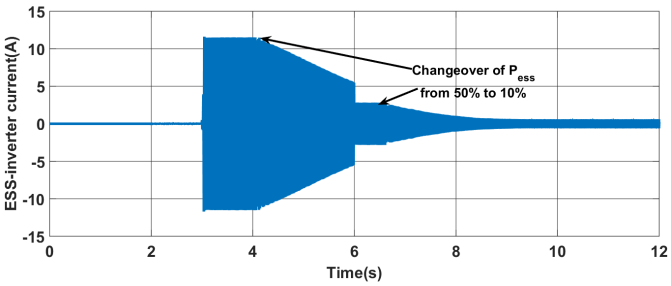


Fig. 13. Phase current dynamics of ESS-inverter during changeover of rating from 50% to 10%

the proposed control algorithm, first only the VSM supplies the load. The frequency dynamics for this case can be observed from Fig. 6. It can be seen that the frequency drops up to 49.39 Hz for J= J_{nom} for VSM of 3 kVA rating. Also, the RoCoF is observed to be 2.71 Hz/s, which can be quite detrimental for the mechanical structure of rotary machines or other electrical equipments. It can be pointed out that as the synchronous machine is modeled with VSM, there is a flexibility over the control of inertia of the machine as depicted in Fig. 6 with two different J values. For a higher value of J, the frequency drop is lesser and RoCoF is better. The governor mechanism of the VSM restores the frequency to nominal value.

Next, the p-q controlled inverter is connected in parallel to the VSM and both participate dynamically to control the frequency. The proposed proportional control algorithm evidently improves the frequency dynamics of the grid as can be observed in Fig. 7. It can be seen clearly that as the rating of the inverter is increased, the frequency profile will have

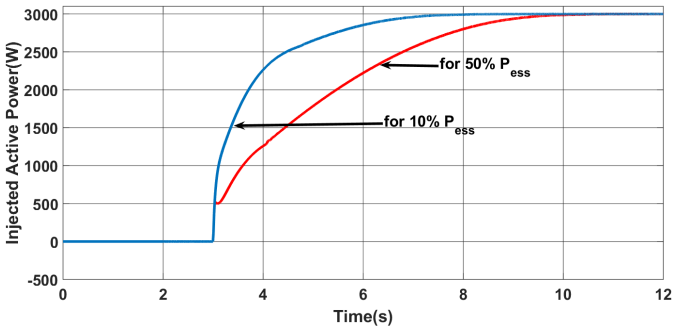


Fig. 11. Power Curve of VSM for different ratings of ESS-inverter

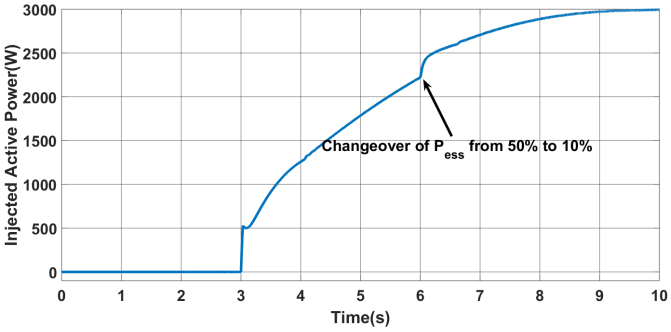


Fig. 14. Peak power handled by VSM during changeover of ESS-inverter from 50% to 10% rating

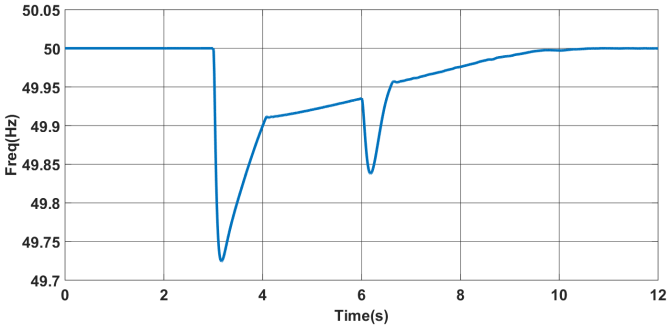


Fig. 15. Frequency dynamics during changeover of ESS-inverter rating from 50% to 10%

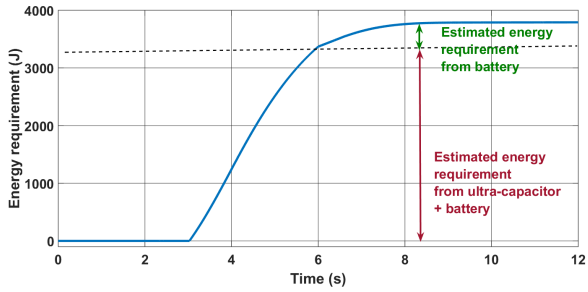


Fig. 16. Estimated energy requirement when changeover of ESS-inverter rating is considered from 50% to 10%

improved dynamics. Here, it should be stated that the nadir of the frequency response depends mostly on the rating of the proposed ESS-inverter. Thus, it is possible to achieve an inertial support to arrest/limit frequency deviations or control RoCoF by properly controlling the inverter with this algorithm. The waveform of modulating signal for VSM control for the case where ESS-inverter rating is chosen 10% of the total system load, is shown in Fig. 8. From the figure, clearly the change in the time period of the modulating signal indicates the change in frequency. The active power shared by the ESS-inverter and the Virtual Synchronous Machine are displayed in Fig. 9 and Fig. 11, respectively. The ESS-inverter is aptly modeled to feed required power during transient condition which decays to zero once the frequency is stabilized to the desired value. The VSM is responsible for supplying the full power demand in steady-state as can be observed from Fig. 11. The time domain plot of phase current of the ESS-inverter for different ratings can be obtained from Fig. 10. It is obvious that the maximum current handled by the inverter is more at a higher rating. Table III lists the comparison of the performance of ESS-inverter for its different ratings to serve the purpose of frequency profile improvement. Thus, the virtual inertial support is enhanced with increase in inverter rating and vice-versa. Here, the percentage of inverter rating is expressed with respect to the total load capacity of the grid that is considered for this study.

Next, few simulation results are displayed to propose a hybrid use of energy storage-mix to combat the frequency deviation. Fig. 12 shows the power curve of the p-q controlled inverter when a switch-over action is adopted to change the

TABLE IV
HARDWARE SYSTEM PARAMETERS

System Parameters	Values
DC Bus voltage	300 V
Load voltage (line-to-line)	165 V (rms)
Load current	5.24 A
Modulation index at no load for VSM	0.9
Filter inductors	7 mH
Switching frequency	4 kHz
Sampling frequency	20 kHz
Nominal value of J of VSM	0.05 kg.m^2
PI gains of the governor (droop control) of VSM	k_p=200, k_i=1000
PI gains of grid voltage controller of VSM	k_p=0.001, k_i=0.01
Proportional gain of the proposed controller	k_p=6000
PI gains of the d-q current controllers	k_p=24, k_i=3200
Load	1.5 kW (resistive)
MOSFET switches	IPP65R110CFD (650 V, 31.2 A)
Battery Bank	300 V, 160 AH

power handling of the inverter from 50% to 10% at 6 seconds. The real essence of this is to propose to utilize available energy storages (ultracapacitors, batteries, etc) properly at appropriate timing instants during any frequency regulation problem. It can be noted from Fig. 12 that the initial active power boost can be achieved by the use of ultra-capacitors along with batteries, which is denoted by the chosen higher initial rating (50%) of the inverter. Once the primary frequency regulation has been initiated, the ultra-capacitors may be cut off from the system and the rest required power can be provided by the battery, which is denoted by the chosen lower rating (10%). Similar effect is observed in case of inverter current in Fig. 13. The transition of delivered-power by the virtual synchronous machine due to the mentioned changeover can be observed in Fig. 14. The effect on system frequency for this changeover can be seen from Fig. 15.

The energy requirement from the energy storage systems can be estimated from Fig. 16. Clearly, energy required for the first half of the response is about 3400J, which can be obtained by having properly designed banks of ultra-capacitors and batteries. This helps to restrict the energy requirement from the battery. From Fig. 12, it is found that battery has supplied a peak power of 250W, while ultacapacitor and battery together are estimated to handle a peak power of about 1400W. If only battery would have been used for the purpose of frequency regulation, the specific energy requirement for a battery bank would have been much more. In this way, the fast transient response property of the ultra-capacitors can be utilized and the battery capacity and cost can also be reduced.

V. EXPERIMENTAL RESULTS

The experimental validation is carried out in the laboratory using dSPACE1103. The set-up of hardware prototype is displayed in Fig. 17. The controller implementation is done with a fixed step size of 50 μs.

The system specification for hardware implementation is listed in Table IV. Three different cases have been considered to show the effectiveness of the algorithm with a step change in resistive load of 1.5 kW. These are: (i) Case-1: System performance with only VSM; (ii) Case-2: System performance with ESS-inverter in parallel with VSM. This experimentation

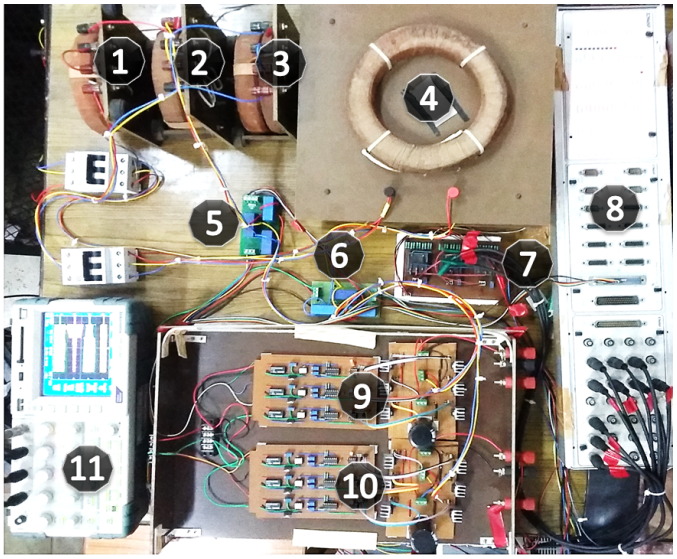


Fig. 17. Hardware prototype: 1,2,3- Coupling inductor for ESS-inverter, 4-coupling inductors for VSM, 5- Current sensor board for ESS-inverter, 6-Current sensor board for VSM, 7- Voltage sensor board, 8- dSPACE1103 controller, 9- ESS-inverter assembly, 10- VSM assembly, 11- Oscilloscope

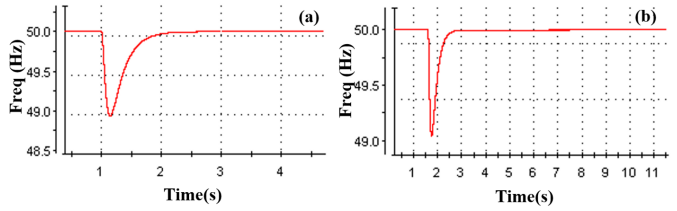


Fig. 18. Experimental results of frequency dynamics with a step change in load. (a)with only VSM, (b)with 10% rated ESS-inverter

is done by limiting the rating of the ESS-inverter to 10%, 50% and 100% of the total load of the system, consecutively; (iii) Case-3: A changeover of the limiter of the ESS-inverter's power injection capability, is made to show the possibility of using two different time-scale energy storage systems.

From Fig. 18, it can be found that with only VSM in the system, the frequency falls upto 49 Hz, whereas with 10% rated ESS-inverter it is improved by 0.2 Hz. With increased energy storage rating, the frequency can be further improved upto 49.55 Hz and 49.75 Hz, for 50% and 100% rating of ESS-inverter, respectively as shown in Fig. 19. It can be easily inferred that the frequency decline which was about 1 Hz without ESS-inverter, can be limited to only 0.25 Hz by

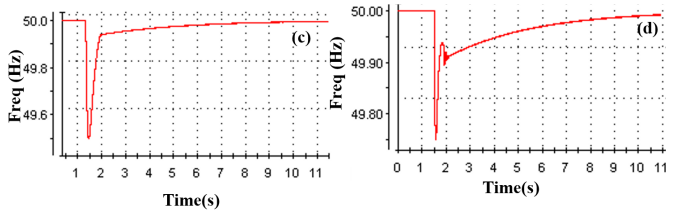


Fig. 19. Experimental results of frequency dynamics with a step change in load. (a)with 50% rated ESS-inverter, (b)with 100% rated ESS-inverter

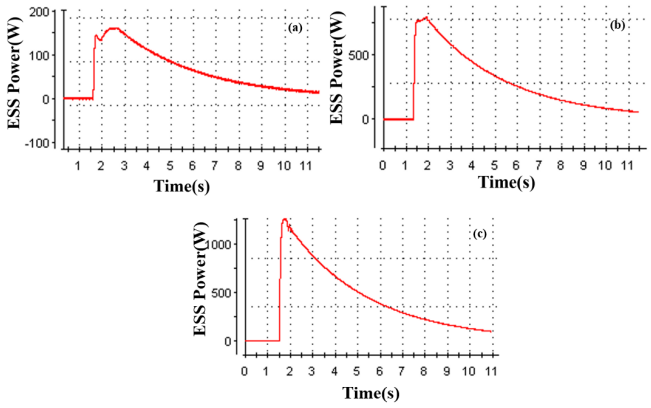


Fig. 20. Experimental results of injected active power by ESS-inverter during step change in load for different ratings respectively, (a)10%, (b)50%, (c)100%

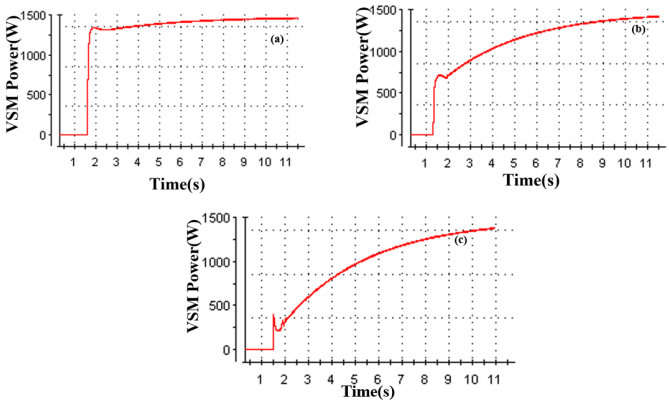


Fig. 21. Experimental results of injected active power by VSM during step change in load for different ratings of ESS-inverter respectively, (a)10%, (b)50%, (c)100%

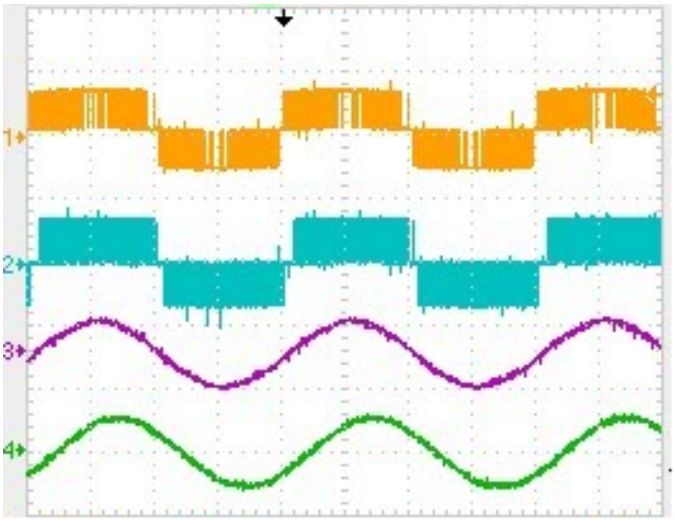


Fig. 22. Oscilloscope waveforms: VSM-Inverter output PWM voltage (CH1, Scale:500 V/div), ESS-Inverter output PWM voltage (CH2, Scale:500 V/div), line-to-line load voltage (CH3, Scale:500 V/div), line current (CH4, Scale:5 A/div), time (Scale: 5 ms/div)

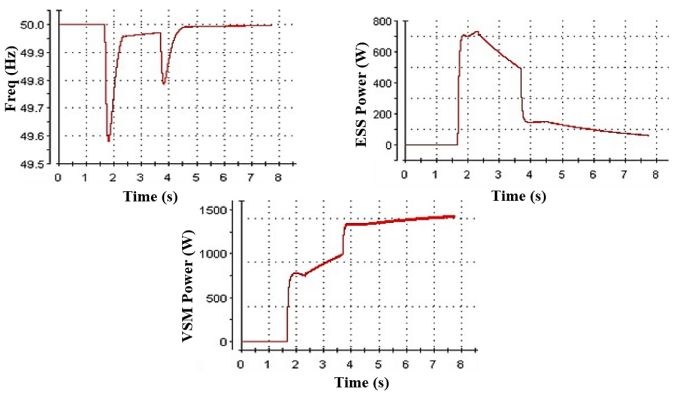


Fig. 23. Experimental results during a changeover of ESS-inverter rating from 50% to 10% at t = 3.5 s. (a) Frequency dynamics, (b) ESS-inverter injected active power, (c) VSM injected active power

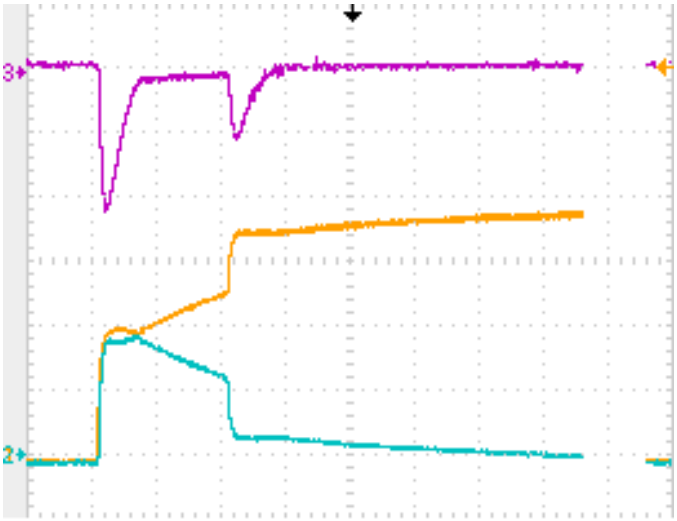


Fig. 24. Oscilloscope waveforms during a changeover of ESS-inverter rating from 50% to 10% at 3.2 s: Injected active power by VSM (CH1, Scale: 400 W/div), Injected active power by ESS inverter (CH2, Scale:400 W/div), frequency profile (CH3, Scale: 0.2 Hz/div), time (Scale: 1 s/div)

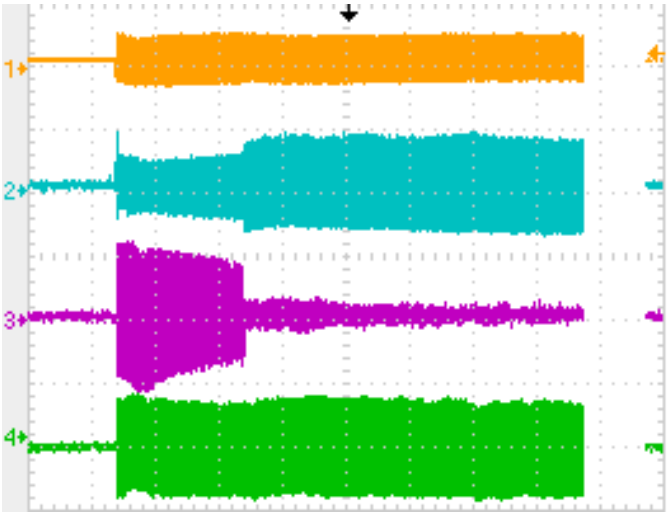


Fig. 25. Oscilloscope waveforms during a changeover of ESS-inverter rating from 50% to 10% at 3.2 s: Voltage across resistive load (CH1, Scale: 500 V/div), Output current of VSM(CH2, Scale:5 A/div), Output current of ESS inverter (CH3, Scale: 2 A/div), Load current(CH4, Scale:5 A/div), time (Scale: 1 s/div)

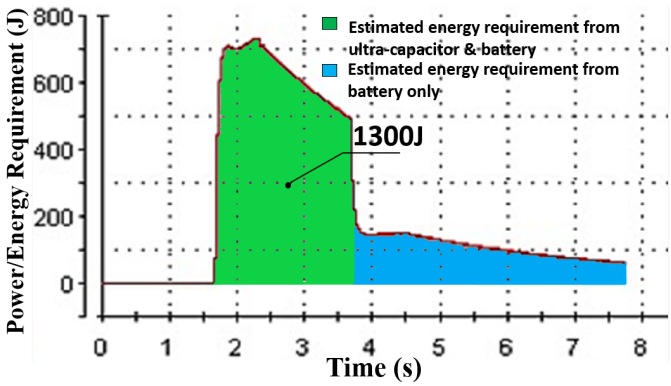


Fig. 26. Indication of estimated energy utilised from ESS during changeover of ESS-inverter rating from 50% to 10% at t = 3.5 s.

utilizing proper rating of energy storage system. Therefore, the rating of ESS has direct impact on how much frequency deviation can be arrested. In essence, the storage system is contributing some synthetic inertia to the system which is guided by its capacity and charging/discharging rates. Fig. 20 and Fig. 21 display the injected active power by the ESS-inverter and the VSM during the instant of load change, respectively. As it can be seen from these experimental results that at any point of time, the sum of the pulsed power supplied by the ESS-inverter and the power supported by the VSM equals the total load power, which is similar to the simulation results as well. The steady-state waveforms of inverter output voltages, line-to-line voltage across load and load current is shown in Fig. 22. To display the potential of the algorithm to switch between different energy storage systems for their optimized utilization, a transition of the power rating of ESS-inverter is carried out from its 50% rating to only 10%. The corresponding waveforms are displayed in Fig. 23. As soon as the load change took place, the ESS-inverter instantly delivered 50% of the total load power, i.e. 750 watts. As a result, the initial power delivered by VSM is also about 750 watts, for a constant load power. Gradually as frequency approached the nominal value, the power output of the ESS-inverter started to decrease and VSM started taking over the load. At t = 3.5 s, the rating of ESS-inverter is switched to 10% which causes a little frequency dip. Afterwards, as the reference current of the ESS-inverter comes out of saturation, the frequency regulation is carried out by VSM which supplies the full load eventually, the output power of ESS-inverter being pulled towards zero. A view of oscilloscope snapshot for this case-study is provided in Fig. 24. It can be found that at around 1 sec, the load change has been made. Consequently, the frequency drops upto nearly 49.55 Hz (for 50% rated ESS-inverter). The ESS-inverter injects 50% of the total load power instantly, while VSM supplies the balance power for a constant load. At 3.2 sec a changeover is made of the ESS-inverter rating from 50% to 10%. This may represent a case when initial power (i.e. 50% of P_{ess}) may be fed by ultra-capacitors and batteries, followed by only batteries when

this changeover is made to 10% of P_{ess}. As a result of the changeover, a small dip (less than 0.05 Hz) in frequency can be observed. Afterwards frequency gradually restores to nominal value. The corresponding dynamics in the power curves of the VSM (CH1) and ESS-inverter (CH2) are also visible from Fig. 24. The corresponding dynamics observed in load voltage, VSM output current, ESS-inverter output current and load current can be observed in Fig. 25. It can be seen that the load voltage is maintained constant and for a constant load current, the ESS current initially picks up and gradually comes down to its 10% rating and finally decays to zero; whereas the VSM current is initially lesser and it gradually picks up to the rated load. The shaded portions in Fig. 26 depict the energy requirement from the ESS which is derived by integrating the power curve of ESS-inverter. As it can be seen from the Fig. 26, that around 1300J may be supplied by combined storage system, comprising ultra-capacitor and battery and the rest (nearly 700J) may be supplied entirely by battery. Hence, more pulsed power may be obtained from fast acting ultra-capacitor storage and as a result, the battery requirement can be curtailed which makes the ESS cost-effective.

VI. Conclusions

This paper has presented the feasibility of a simple control technique to enhance the dynamic behavior of the microgrid with respect to frequency response. It is shown that a simple proportional gain based controller together with proper selection of current-limits can inject the required active power demand during any kind of load variations. Understanding that the estimation of system-frequency is extremely difficult during the transients, a new frequency estimation technique based on VSM-speed is demonstrated. This helps to avoid the time delay problems encountered in the measurement of system-frequency using PLL. The proposed system is extensively simulated in MATLAB/Simulink. An experimental prototype is developed in the laboratory and experimental results support the validation of the proposed control technique, confirming the usefulness of the proposed concepts. The results show that the proposed frequency controller is simple and efficient for primary frequency regulation. For proper implementation of the proposed algorithm, optimal sizing of energy storage is required depending on the variability of the injected power. Also, optimal use of different storage mix, such as battery, ultra-capacitors, or pumped storage system, needs to be explored for optimization of energy storage system.

Acknowledgment

The authors would like to acknowledge financial support received from Department of Science & Technology (DST), India through a project entitled UK India Clean Energy Research Institute (UKICERI) (DST/RCUK/JVCCE/2015/02 (C)), and EPSRC funded Joint Clean Energy Research Centre (JUICE) (EP/P003605/1) which is a joint collaboration initiative between DST, India and EPSRC, UK.

References

[1] S. D'Arco, J. A. Suul, and O. B. Fosso, "A virtual synchronous machine implementation for distributed control of power converters in smartgrids," *Electric Power Systems Research*, vol. 122, pp. 180 – 197, 2015.

[2] W. Zhang, D. Remon, and P. Rodriguez, "Frequency support characteristics of grid-interactive power converters based on the synchronous power controller," *IET Renewable Power Generation*, vol. 11, no. 4, pp. 470–479, 2017.

[3] A. A. Renjit, F. Guo, and R. Sharma, "An analytical framework to design a dynamic frequency control scheme for microgrids using energy storage," in *2016 IEEE Applied Power Electronics Conference and Exposition (APEC)*, March 2016, pp. 1682–1689.

[4] G. Delille, B. Francois, and G. Malarange, "Dynamic frequency control support by energy storage to reduce the impact of wind and solar generation on isolated power system's inertia," *IEEE Transactions on Sustainable Energy*, vol. 3, no. 4, pp. 931–939, Oct 2012.

[5] T. Xu, W. Jang, and T. Overbye, "Commitment of fast-responding storage devices to mimic inertia for the enhancement of primary frequency response," *IEEE Transactions on Power Systems*, vol. 33, no. 2, pp. 1219–1230, March 2018.

[6] E. Rakhshani and P. Rodriguez, "Inertia emulation in ac/dc interconnected power systems using derivative technique considering frequency measurement effects," *IEEE Transactions on Power Systems*, vol. 32, no. 5, pp. 3338–3351, Sept 2017.

[7] D. Wu, F. Tang, T. Dragicevic, J. M. Guerrero, and J. C. Vasquez, "Coordinated control based on bus-signaling and virtual inertia for islanded dc microgrids," *IEEE Transactions on Smart Grid*, vol. 6, no. 6, pp. 2627–2638, Nov 2015.

[8] N. Soni, S. Doolla, and M. C. Chandorkar, "Inertia design methods for islanded microgrids having static and rotating energy sources," *IEEE Transactions on Industry Applications*, vol. 52, no. 6, pp. 5165–5174, Nov 2016.

[9] M. Guan, W. Pan, J. Zhang, Q. Hao, J. Cheng, and X. Zheng, "Synchronous generator emulation control strategy for voltage source converter (vsc) stations," *IEEE Transactions on Power Systems*, vol. 30, no. 6, pp. 3093–3101, Nov 2015.

[10] J. A. Suul, S. D'Arco, and G. Guidi, "Virtual synchronous machine-based control of a single-phase bi-directional battery charger for providing vehicle-to-grid services," *IEEE Transactions on Industry Applications*, vol. 52, no. 4, pp. 3234–3244, July 2016.

[11] P. F. Frack, R. W. D. Doncker, P. E. Mercado, and M. G. Molina, "Emulation of synchronous machine for frequency stability improvement in microgrids," in *2015 IEEE 11th International Conference on Power Electronics and Drive Systems*, June 2015, pp. 59–66.

[12] P. Zarina, S. Mishra, and P. Sekhar, "Exploring frequency control capability of a pv system in a hybrid pv-rotating machine-without storage system," *International Journal of Electrical Power & Energy Systems*, vol. 60, pp. 258 – 267, 2014.

[13] W. S. Im, C. Wang, W. Liu, L. Liu, and J. M. Kim, "Distributed virtual inertia based control of multiple photovoltaic systems in autonomous microgrid," *IEEE/CAA Journal of Automatica Sinica*, vol. 4, no. 3, pp. 512–519, 2017.

[14] X. Xi, H. Geng, G. Yang, S. Li, and F. Gao, "Two-level damping control for dfig-based wind farm providing synthetic inertial service," *IEEE Transactions on Industry Applications - Early Access*, 2017.

[15] R. Engleitner, A. Nied, M. S. M. Cavalca, and J. P. da Costa, "Dynamic analysis of small wind turbines frequency support capability in a low-power wind-diesel microgrid," *IEEE Transactions on Industry Applications*, vol. 54, no. 1, pp. 102–111, Jan 2018.

[16] J. Zhu, J. Hu, W. Hung, C. Wang, X. Zhang, S. Bu, Q. Li, H. Urdal, and C. D. Booth, "Synthetic inertia control strategy for doubly-fed induction generator wind turbine generators using lithium-ion supercapacitors," *IEEE Transactions on Energy Conversion - Early Access*, 2017.

[17] J. Zhu, C. D. Booth, G. P. Adam, A. J. Roscoe, and C. G. Bright, "Inertia emulation control strategy for vsc-hvdc transmission systems," *IEEE Transactions on Power Systems*, vol. 28, no. 2, pp. 1277–1287, May 2013.

[18] M. Zhang, X. Yuan, and J. Hu, "Inertia and primary frequency provisions of pll-synchronized vsc hvdc when attached to islanded ac system," *IEEE Transactions on Power Systems - Early Access*, 2017.

[19] L. M. Castro and E. Acha, "On the provision of frequency regulation in low inertia ac grids using hvdc systems," *IEEE Transactions on Smart Grid*, vol. 7, no. 6, pp. 2680–2690, Nov 2016.

[20] S. Pulendran and J. E. Tate, "Energy storage system control for prevention of transient under-frequency load shedding," *IEEE Transactions on Smart Grid*, vol. 8, no. 2, pp. 927–936, March 2017.
[21] J. Fang, Y. Tang, H. Li, and X. Li, "A battery/ultracapacitor hybrid energy storage system for implementing the power management of virtual synchronous generators," *IEEE Transactions on Power Electronics*, vol. 33, no. 4, pp. 2820–2824, April 2018.
[22] U. Bose, S. K. Chattopadhyay, C. Chakraborty, and B. Pal, "A novel method of frequency regulation in microgrid," in *2016 IEEE 7th Power India International Conference (PIICON)*, Nov 2016, pp. 1–6.
[23] R. Teodorescu, M. Liserre, and P. Rodriguez, *Grid Converters for Photovoltaic and Wind Power Systems*. Wiley, 2011.
[24] P. Kundur, N. Balu, and M. Lauby, *Power System Stability and Control*, ser. Discussion Paper Series. McGraw-Hill Education, 1994.
[25] X. Wang, M. Yue, and E. Muljadi, "Pv generation enhancement with a virtual inertia emulator to provide inertial response to the grid," in *2014 IEEE Energy Conversion Congress and Exposition (ECCE)*, Sept 2014, pp. 17–23.
[26] H. A. Alsiraji and R. El-Shatshat, "Comprehensive assessment of virtual synchronous machine based voltage source converter controllers," *IET Generation, Transmission Distribution*, vol. 11, no. 7, pp. 1762–1769, 2017.
[27] B. Wu, Y. Lang, N. Zargari, and S. Kouro, *Power Converters in Wind Energy Conversion Systems*. Wiley-IEEE Press, 2011, p. 480.



Upama Bose (S'17) received her B.Tech. degree in Electrical Engineering from Narula Institute of Technology, Kolkata, India and M. Tech Degree in Electrical Engineering with specialization in Power Electronics and Drives from Vellore Institute of Technology, Vellore, India in the year 2012 and 2015 respectively. She is currently pursuing her PhD in the Department of Electrical Engineering, Indian Institute of Technology Kharagpur. Her research interests include power electronic converters, renewable energy and microgrids.



Sumit K. Chattopadhyay (M'17) received his B.E. degree in Electrical Engineering from Burdwan University, Burdwan, India, in 2004 and M.Tech. degree in Industrial Electrical Systems from the National Institute of Technology Durgapur in 2006. He has nearly 5 years of industrial experience working in the areas of Power Electronic converters for Renewable Energy, Naval applications and HVDC. He has proposed a new series of Multi Level Inverter Topology using Level Doubling Network. He served Larsen & Toubro Ltd as Power Electronic System Designer at Navi Mumbai, India for more than three years. He worked in L&T until January 2010.

From January 2010 to March 2015, he was a full-time Research Scholar with the Department of Electrical Engineering, IIT Kharagpur. There he worked on multilevel inverter topology, modulation, control and applications. From March 2015 to July 2016 he has served as Scientist of HVDC Grid System R&D with ABB Global Industries Service Ltd. in India. He was a Post-doctoral Fellow in the Dept. of Electrical Engineering of IIT Kharagpur form July 2016 to June 2018. Currently he is working as an Assistant Professor at Centre for Energy Studies in IIT Delhi.



Chandan Chakraborty (S'92-M'97-SM'01-F'15) received B.E and M.E degrees in Electrical Engineering from Jadavpur University in 1987 and 1989 respectively and Ph.D degrees from Indian Institute of Technology Kharagpur and Mie University, Japan in 1997 and 2000 respectively. Presently, he is a professor in the Department of Electrical Engineering, Indian Institute of Technology Kharagpur. His research interest includes power converters, motor drives, electric vehicles and renewable energy.

Dr. Chakraborty was awarded the JSPS Fellowship to work at the University of Tokyo during 2000-2002. He has received the Bimal Bose award in power electronics in 2006 from the IETE (India). He has regularly contributed to IES conferences such as IECON, ISIE and ICIT as technical program chair/track chair. He is an ADCOM member of the IEEE Industrial Electronics Society. He is one of the Associate Editors of IEEE Transactions on Industrial Electronics and IEEE Industrial Electronics Magazine and an Editor of the IEEE Transactions on Sustainable Energy. He is the Founding Editor-in-Chief of IE Technology News (ITeN), a web-only publication for IEEE Industrial Electronics Society. He is a Fellow of IEEE and Indian National Academy of Engineering (INAE).



Bikash C. Pal (M'00-SM'02-F'13) recieved the B.E.E. (with honors) degree from Jadavpur University, Calcutta, India, M.E. degree from the Indian Institute of Science, Bangalore, India, and Ph.D. degree from Imperial College London, London, U.K, in 1990, 1992, and 1999, respectively, all in electrical engineering.

Currently, he is a Professor with the Department of Electrical and Electronic Engineering, Imperial College London. He was Editor-in-Chief of IEEE Transactions on Sustainable Energy (2012-2017) and Editor-in-Chief of IET Generation, Transmission and Distribution (2005-2012) and is Fellow of IEEE for his contribution to power system stability and control. His current research interests include renewable energy modelling and control, state estimation, and power system dynamics.